Hybrid Integration Scheme for the Evaluation of Strongly Singular and Near-Singular Integrals in Surface Integral Equations

Hybrid Integration Scheme for the Evaluation of Strongly Singular and Near-Singular Integrals in Surface Integral Equations

J. Rivero, F. Vipiana, *Senior Member, IEEE*, D. R. Wilton, *Life Fellow, IEEE*, and W. A. Johnson, *Senior Member, IEEE*

***Abstract*—The accurate and efficient evaluation of surface source integrals is a key step in obtaining reliable solutions of electromagnetic problems using integral equation formulations. In this paper, we propose to combine two of the most extensively used schemes to efficiently evaluate strongly singular and near-singular source integrals, such as those arising in the $\mathcal{K}$ operator. In the proposed approach, singularity subtraction is first applied to remove the most dominant singular part; singularity cancellation, using the radial-angular variable transformation, is then employed to treat the remaining integrand. The method is compared to other common numerical schemes to demonstrate its effectiveness.**

***Index Terms*—Integral equations, moment methods, singular integrals, numerical analysis.**

I. Introduction

The rigorous solution of radiation and scattering problems using surface integral equation formulations solved via the Method of Moments (MoM) requires the accurate and efficient numerical evaluation of singular and near-singular double surface integrals. Here, we focus on the numerical solution of the double integrals involving the gradient of the Green's function, usually called *strongly* singular and near-singular integrals, whose kernel has a singularity of the kind $1/R^2$ [1]. This double surface integral operator, widely known also as the $\mathcal{K}$ operator [2], arise in both the Magnetic Field Integral Equation (MFIE), the Combined Field Integral Equation (CFIE) for perfect electric conductor (PEC), as well as in the commonly used formulations for penetrable bodies (dielectrics, homogenized metamaterials, plasmonic bodies, etc.) such as the classical Poggio-Miller-Chan-Harrington-Wu-Tsai (PMCHWT) formulation and other combined formulations.

The evaluation of the source surface integral has been traditionally accomplished by applying well-known "singularity subtraction" integration schemes [3], [4]. The basic idea of a singularity subtraction integration scheme is to subtract from the integrand terms that have the same asymptotic behavior as the integrand at its singularities. The remaining (smoothed) integrand is then numerically evaluated using a standard quadrature scheme. Then, the subtracted singular terms are integrated analytically and added back into the final result. Usually, the singularity subtraction integration schemes are able to provide low-to-medium accuracy (up to 7-8 correct significant digits for the MFIE) with only a few quadrature sample points, thanks to the dominant contribution of the exactly integrated analytical part. However, the maximum attainable accuracy is limited by the numerical evaluation of the regularized integral, which may still contain lower order singularities of either the unbounded or bounded type, as is especially true for the $\mathcal{K}$ operator on curvilinear domains [5].

A more recent approach, alternative to the singularity subtraction scheme, employs the so-called "singularity cancellation" method [6]–[9]. In singularity cancellation schemes, the singularities are cancelled through a proper sequence of variable transformations; the resulting integral is then evaluated numerically with a standard quadrature scheme. Singularity cancellation schemes are basically independent of the basis function kind and order, and of the integration domain shape and curvature. Moreover, it is possible for well-designed schemes to achieve machine precision by merely increasing the quadrature order. However, in the low-to-medium accuracy regime, more sample integration points are generally needed than in the singularity subtraction scheme [5]. Finally, for the MFIE (or $\mathcal{K}$ operator), a complex subdivision of the integration domain is often required to accurately evaluate the contribution of a principal value integral [8]. We remark that machine precision accuracy for computations in a production code is both unnecessary and expensive. But the ability to generate good reference values and not to be *limited* by the attainable precision are strong reasons for desiring high accuracy. Furthermore, some types of problems benefit from simply increasing the accuracy. These include, for example, the computation of mode dispersion diagrams for waveguiding structures, the validation of implementations of higher order bases, and countering effects of ill-conditioning. Problems requiring large dynamic ranges, such as the computation of low sidelobe levels in antenna or scattering patterns also benefit from higher accuracy.

Usually, in the MoM, a two step procedure is used to evaluate source and testing moment integrals. In the first, the source integral is treated rather carefully, and in the second,

Manuscript received xxxxxxx, 2018.

J. Rivero and F. Vipiana are with the Department of Electronics and Telecommunications, Politecnico di Torino, 10129 Torino, Italy (email: {javier.rivero, francesca.vipiana}@polito.it).

D. R. Wilton is with the Department of Electrical and Computer Engineering, University of Houston, Houston, TX 77204-4005 USA (email: wilton@uh.edu).

W. A. Johnson is an electromagnetics consultant in Albuquerque, NM 87123, USA (e-mail: w.johnson24@comcast.net).

Color versions of one or more of the figures in this communication are available online at http://ieeexplore.ieee.org.

Digital Object Identifier xxxxxxxxxxxxxxxxxxxx

the resulting source integral is assumed sufficiently smooth that it can be integrated (tested) numerically using a standard low-order quadrature scheme. Recently, however, a number of methods have emerged for dealing simultaneously with the two surface integrals for the various kernels encountered in the MoM [10]–[15]. These methods are mainly based on applying the divergence theorem to both the source and test surface integrals, together with an appropriate reordering of the obtained radial and contour integrals. Though promising, these methods are currently still in development; they also require significant changes to existing MoM code implementations, and hence are not yet in wide use.

In this paper, we propose a novel integration scheme, called the *hybrid integration scheme* in the following, that properly combines the singularity subtraction and cancellation approaches so as to minimize the number of quadrature points for low-to-medium accuracy, while still being able to reach machine precision as the number of quadrature points is increased. The proposed hybrid integration scheme is easily applied to flat and curvilinear (quadratic) triangular integration domains, and for observation points near or on the integration surface or edges. The present paper is partly inspired by a comment on how to treat the remaining $1/R$ singularity after subtracting higher order singularities, mentioned in [16] for the case of flat triangular domains.

The paper is organized as follows. Sect. II describes the proposed formulation for the evaluation of the gradient of the Green's function present in the MoM discretization of the MFIE for planar triangles. In Sect. III, the extension to curvilinear triangles is detailed. Numerical results are then presented in Sect. IV. Finally, Sect. V contains the conclusion and perspectives. Preliminary results for the proposed approach were presented in [17].

II. The Hybrid Integration Scheme

The aim of this paper is to develop an accurate and efficient evaluation of strongly singular and near-singular integrals, e.g. those present in the source integral of the MFIE, discretized via the MoM. Such integrals have the form

$$\begin{aligned}\mathbf{I}_n(\mathbf{r}) &= \iint_{\mathcal{T}'} \boldsymbol{\nabla}\frac{e^{-jkR}}{4\pi R}\times\boldsymbol{\Lambda}_n(\mathbf{r}')dS' \\ &= \iint_{\mathcal{T}'} \boldsymbol{\Lambda}_n(\mathbf{r}')(1+jkR)e^{-jkR}\times\frac{\mathbf{R}}{4\pi R^3}dS', \quad (1)\end{aligned}$$

where k is the wavenumber, $\mathbf{R}=\mathbf{r}-\mathbf{r}'$, $R=|\mathbf{R}|$, $\mathbf{r}$ is an observation point, $\mathbf{r}'$ is a source point on the triangle $\mathcal{T}'$, and $\boldsymbol{\Lambda}_n$ is the n-th basis function as, e.g., a Rao-Wilton-Glisson (RWG) basis function [18]. A RWG basis function, $\boldsymbol{\Lambda}_n(\mathbf{r}')$ is defined on the triangle $\mathcal{T}'$ as

$$\boldsymbol{\Lambda}_n(\mathbf{r}') = \frac{\boldsymbol{\rho}_n}{h_n} = \frac{\mathbf{r}'-\mathbf{r}_n}{h_n}, \quad (2)$$

where $\mathbf{r}_n$ is the triangle vertex associated with the considered n-th basis function, and h_n is the corresponding triangle height, as shown in Fig. 1. We observe that the integral in (1) has an asymptotic behavior of $1/R^2$ as $R\to 0$.

In this work, we propose a novel hybrid integration scheme able to evaluate singular and near-singular integrals of the kind in (1) that combines the advantages of the singularity subtraction and cancellation methods mentioned in Sect. I.

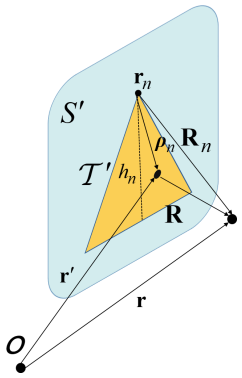

Fig. 1. Integration domain and relevant geometrical quantities.

In the proposed approach, we first write (1) as

$$\mathbf{I}_n(\mathbf{r}) = -\frac{1}{4\pi}\iint_{\mathcal{T}'}\mathbf{R}_n\times\boldsymbol{\Lambda}_n\frac{(1+jkR)e^{-jkR}}{R^3}dS', \quad (3)$$

observing that $\boldsymbol{\Lambda}_n\times\mathbf{R}=\boldsymbol{\Lambda}_n\times(\mathbf{R}_n-\boldsymbol{\rho}_n)=-\mathbf{R}_n\times\boldsymbol{\Lambda}_n$ since, by (2), $\boldsymbol{\Lambda}_n\propto\boldsymbol{\rho}_n$. Then, we subtract the term $\mathbf{R}_n\times\boldsymbol{\Lambda}_n/R^3$ from the integrand of (3), and add its surface integral to the result, obtaining

$$\mathbf{I}_n(\mathbf{r}) = \mathbf{I}_n^R(\mathbf{r}) + \mathbf{I}_n^{R^3}(\mathbf{r}), \quad (4)$$

where

$$\mathbf{I}_n^R(\mathbf{r}) = -\frac{1}{4\pi}\iint_{\mathcal{T}'}\mathbf{R}_n\times\boldsymbol{\Lambda}_n\frac{(1+jkR)e^{-jkR}-1}{R^3}dS' \quad (5)$$

$$\mathbf{I}_n^{R^3}(\mathbf{r}) = -\frac{1}{4\pi}\iint_{\mathcal{T}'}\mathbf{R}_n\times\boldsymbol{\Lambda}_n(\mathbf{r}')\frac{1}{R^3}dS'. \quad (6)$$

A most important feature of (6) is that it can be evaluated analytically as in [3]. To guard against the cancellation error that can occur for small kR, we replace the exponential function in the kernel of (5) by its appropriately truncated Maclaurin series expansion in kR, and cancel the leading static term analytically rather than rely on numerical cancellation.

In contrast to (1), which has a $1/R^2$ singularity, the integral (5) has only a $1/R$ behavior as $R\to 0$, and can be evaluated by the radial-angular singularity cancellation scheme presented in [19]. It is worth noting that the radial-angular transform appears to be among the most effective singularity cancellation schemes [20].

In order to apply the radial-angular transform, the observation point $\mathbf{r}$ is projected onto the triangle $\mathcal{T}'$ plane, as illustrated in Fig. 2a. The triangle $\mathcal{T}'$ is then split into three sub-triangles about the projected observation point. Fig. 2b shows one sub-triangle with a local reference system and with the origin at the projected observation point. If the observation point is off the surface but with its projection in $\mathcal{T}'$, the dominant contributions are generally additive. But if the projected observation point is exterior to $\mathcal{T}'$, those sub-triangles that are fully exterior to $\mathcal{T}'$ have negative contributions whose dominant contributions should exactly cancel, and can induce cancellation errors for large triangle/observation

point separations. Thus as we move further from the triangle, we should simply do the smooth integrals numerically.

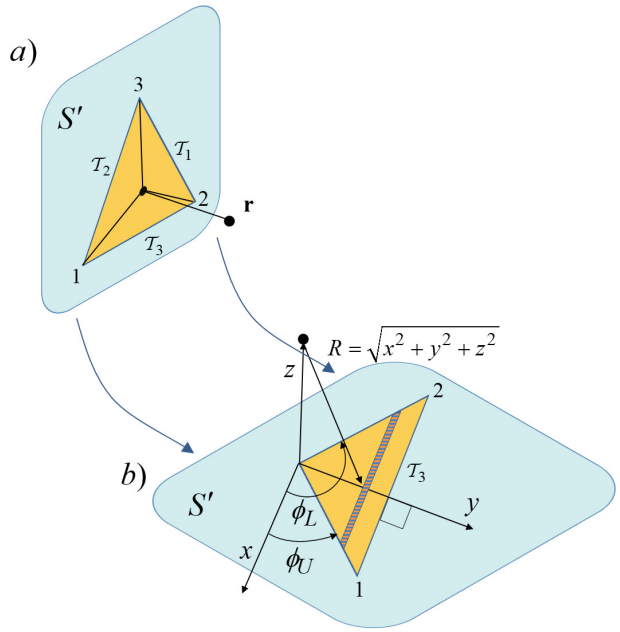

Fig. 2. Application of the singularity cancellation scheme via triangle splitting; (a): original triangular domain split into three sub-triangles; (b): one sub-triangles and corresponding relevant geometrical quantities.

Then, the integral (5) can be rewritten as

$$\mathbf{I}_n^R = \mathbf{I}_n^{\mathcal{T}_1} + \mathbf{I}_n^{\mathcal{T}_2} + \mathbf{I}_n^{\mathcal{T}_3}, \tag{7}$$

where

$$\mathbf{I}_n^{\mathcal{T}_i} = \int_0^h dy \int_{x_L}^{x_U} dx\, \mathbf{g}_n(x,y) \tag{8}$$

with $x_U = y\cot(\phi_U)$ and $x_L = y\cot(\phi_L)$; ϕ_U and ϕ_L are the minimum and maximum aperture angle of the considered sub-triangle respectively, as shown in Fig. 2b, h is the height of the sub-triangle along the y axis, and $\mathbf{g}_n(x,y)$ represents the integrand of (5). Applying the radial-angular transform, (8) becomes

$$\mathbf{I}_n^{\mathcal{T}_i} = \int_{u_L}^{u_U} du \int_{v_L}^{v_U} dv\, \mathbf{g}_n[x(u,v), y(u,v)]\, \mathcal{J}(u,v), \tag{9}$$

where

$$\begin{aligned} u &= \ln\tan\frac{\phi}{2} \quad \text{with} \quad \phi = \arctan\frac{y}{x} \\ v &= R = \sqrt{x^2+y^2+z^2}, \end{aligned} \tag{10}$$

the integration limits are

$$\begin{aligned} u_{L,U} &= \ln\tan\frac{\phi_{L,U}}{2} \\ v_{L,U} &= |z|, \sqrt{z^2+(h\cosh u)^2}, \end{aligned} \tag{11}$$

and the Jacobian is

$$\mathcal{J} = \frac{R}{\cosh u}. \tag{12}$$

Using the radial-angular transform, the Jacobian (12) exactly cancels the static part of the kernel $1/R$, and maps the sub-triangle into a (almost) rectangular domain, so that Gauss-Legendre integration quadrature schemes of low order can be used to get high accuracy evaluations [19].

III. Extension to Curvilinear Triangles

The proposed integration scheme (Sect. II) can be easily extended to the case when the definition domain $\mathcal{T}'$ of the basis function $\mathbf{\Lambda}_n(\mathbf{r}')$ is a curvilinear triangle. For simplicity, and without loss of generality, here we illustrate the approach for a quadratic triangle.

First, the integral (1) is rewritten in *area* coordinates $\boldsymbol{\xi} = (\xi_1, \xi_2, \xi_3)$, with $\xi_1 + \xi_2 + \xi_3 = 1$,

$$\begin{aligned} \mathbf{I}_n(\mathbf{r}) &= \frac{1}{4\pi}\int_0^1 d\xi_2 \int_0^{1-\xi_2} d\xi_1 \mathbf{\Lambda}_n(\mathbf{r}'(\boldsymbol{\xi})) \\ &\quad (1+jkR(\boldsymbol{\xi}))e^{-jkR(\boldsymbol{\xi})} \times \frac{\mathbf{R}(\boldsymbol{\xi})}{R(\boldsymbol{\xi})^3}\mathcal{J}(\boldsymbol{\xi}), \end{aligned} \tag{13}$$

where $\mathbf{R}(\boldsymbol{\xi}) = \mathbf{r} - \mathbf{r}'(\boldsymbol{\xi})$, $R(\boldsymbol{\xi}) = |\mathbf{R}(\boldsymbol{\xi})|$, and, for a quadratic triangle, the point $\mathbf{r}'(\boldsymbol{\xi})$ on the curvilinear triangle can be written in area coordinates as

$$\begin{aligned} \mathbf{r}'(\boldsymbol{\xi}) &= \mathbf{r}_{020}\, 2\,\xi_2\left(\xi_2 - \frac{1}{2}\right) + \mathbf{r}_{011}\, 4\,\xi_2\,\xi_3 \\ &+ \mathbf{r}_{110}\, 4\,\xi_1\,\xi_2 + \mathbf{r}_{002}\, 2\,\xi_3\left(\xi_3 - \frac{1}{2}\right) \\ &+ \mathbf{r}_{101}\, 4\,\xi_1\,\xi_3 + \mathbf{r}_{200}\, 2\,\xi_1\left(\xi_1 - \frac{1}{2}\right) \end{aligned} \tag{14}$$

In (14), $\mathbf{r}_{ijk}$ with $i,j,k = 0,1,2$ are the coordinates of the six points that identify a curvilinear (quadratic) triangle, as shown in Fig. 3a, according to the multi-index notation introduced in [21]. We note that the mapping is from the parametric space of Fig. 3b to the curvilinear space of Fig. 3a.

Moreover, the extension to curvilinear triangles of the RWG basis functions can be easily written in area coordinates as

$$\mathbf{\Lambda}_n(\mathbf{r}'(\boldsymbol{\xi})) = \frac{\xi_{n+1}\boldsymbol{\ell}_{n-1}(\boldsymbol{\xi}) - \xi_{n-1}\boldsymbol{\ell}_{n+1}(\boldsymbol{\xi})}{\mathcal{J}(\boldsymbol{\xi})}, \qquad n = 1,2,3, \tag{15}$$

where the index arithmetic is performed modulo 3, $\mathcal{J}(\boldsymbol{\xi}) = |\boldsymbol{\ell}_1(\boldsymbol{\xi}) \times \boldsymbol{\ell}_2(\boldsymbol{\xi})|$ and $\boldsymbol{\ell}_n$ are the tangent triangle vectors

$$\boldsymbol{\ell}_n(\boldsymbol{\xi}) = \frac{\partial \mathbf{r}'(\boldsymbol{\xi})}{\partial \xi_{n-1}} - \frac{\partial \mathbf{r}'(\boldsymbol{\xi})}{\partial \xi_{n+1}}, \qquad n = 1,2,3, \tag{16}$$

with $\boldsymbol{\ell}_1 + \boldsymbol{\ell}_2 + \boldsymbol{\ell}_3 = \mathbf{0}$.

Then, we consider a flat triangle, $\mathcal{T}'_T$, *tangent* to the curvilinear one at the projection of the observation point onto the curvilinear triangle, $\mathbf{r}_0 = \mathbf{r}'(\boldsymbol{\xi}_0)$, as shown in Fig. 4. We notice that the definition of the tangent triangle is related to the chosen observation point $\mathbf{r}$, i.e. there is a different tangent triangle for each observation point $\mathbf{r}$. The three vertices of the tangent triangle $\mathcal{T}'_T$ can be expressed as

$$\mathbf{r}_n^0 = \mathbf{r}_0 + \xi_{n-1}^0 \boldsymbol{\ell}_{n+1}(\boldsymbol{\xi}_0) - \xi_{n+1}^0 \boldsymbol{\ell}_{n-1}(\boldsymbol{\xi}_0), \quad n = 1,2,3, \tag{17}$$

where $\boldsymbol{\xi}_0 = (\xi_1^0, \xi_2^0, \xi_3^0)$ is the area coordinate vector of the projected observation point $\mathbf{r}_0$, and $\boldsymbol{\ell}_n(\boldsymbol{\xi}_0)$ are the element tangent vectors (16) evaluated at $\boldsymbol{\xi}_0$, and which are also edge

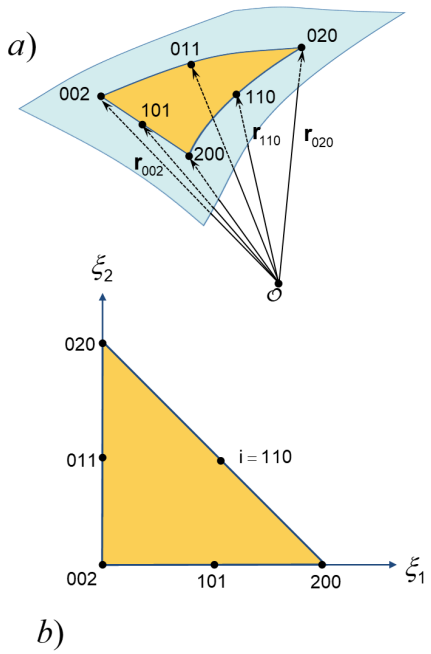

Fig. 3. (a): curvilinear triangle and relevant geometrical quantities; (b): curvilinear triangle mapped in the area coordinate domain.

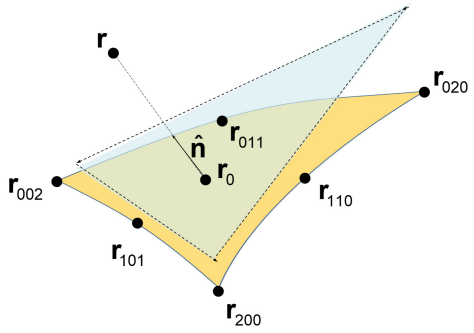

Fig. 4. Curvilinear triangle and corresponding flat tangent triangle at the projected observation point $\mathbf{r}_0$.

vectors of the tangent triangle. We further observe that the defined tangent triangle $\mathcal{T}'_T$ has both the same area coordinates and the same Jacobian at the tangent point $\boldsymbol{\xi}_0$ as the curvilinear one $\mathcal{T}'$. Finally, due to (17), the curvilinear RWG basis functions (15), at the tangent point $\mathbf{r}_0$, are the same as the (ordinary) RWG basis function (2) defined on the tangent triangle [22].

As for the flat case (Sect. II), to smooth the singularity of the integral (13), we subtract and add a term with the same dominant asymptotic behavior as the integrand:

$$\mathbf{I}_n(\mathbf{r}) = \mathbf{I}_n^R(\mathbf{r}) + \mathbf{I}_n^{R^3}(\mathbf{r}) \tag{18}$$

where

$$\mathbf{I}_n^R(\mathbf{r}) = \frac{1}{4\pi}\int_0^1 d\xi_2 \int_0^{1-\xi_2} d\xi_1 \left[\boldsymbol{\Lambda}_{\mathbf{n}}(\mathbf{r}')(1+jkR)e^{-jkR} \times \frac{\mathbf{R}}{R^3}\mathcal{J}(\boldsymbol{\xi}) - \mathbf{F}_n\left(\tilde{\mathbf{r}}'(\boldsymbol{\xi})\right)\mathcal{J}(\boldsymbol{\xi}_0)\right] \tag{19}$$

$$\mathbf{I}_n^{R^3}(\mathbf{r}) = \frac{1}{4\pi}\int_0^1 d\xi_2 \int_0^{1-\xi_2} d\xi_1 \mathbf{F}_n\left(\tilde{\mathbf{r}}'(\boldsymbol{\xi})\right)\mathcal{J}(\boldsymbol{\xi}_0) \tag{20}$$

$$\mathbf{F}_n(\tilde{\mathbf{r}}'(\boldsymbol{\xi})) = -\mathbf{R}_n \times \boldsymbol{\Lambda}_{\mathbf{n}}\left(\tilde{\mathbf{r}}'(\boldsymbol{\xi})\right)\frac{1}{|\mathbf{r}-\tilde{\mathbf{r}}'(\boldsymbol{\xi})|^3}, \tag{21}$$

with $\mathbf{R}_n = \mathbf{r} - \mathbf{r}_n^0$ (17) and $\tilde{\mathbf{r}}'(\boldsymbol{\xi}) = \xi_1\mathbf{r}_1^0 + \xi_2\mathbf{r}_2^0 + \xi_3\mathbf{r}_3^0$.

In (18), the subtracted and summed term is of the same form as in the case of a flat triangular integration domain (4), but, here, it is evaluated on the flat tangent triangle $\mathcal{T}'_T$; in fact, the points $\tilde{\mathbf{r}}'$ are the area coordinate points $\boldsymbol{\xi}$ mapped onto the flat tangent triangle. Hence, we are not introducing an approximation in the evaluation of the initial integral defined over a curvilinear domain. I.e., though the subtracted and added term only approximates the integrand, the singularity is removed because the approximation becomes asymptotically exact as the kernel singularity is approached. In this way, the integral (20) can be easily rewritten as

$$\mathbf{I}_n^{R^3}(\mathbf{r}) = -\frac{1}{4\pi}\iint_{\mathcal{T}'_T} \mathbf{R}_n \times \boldsymbol{\Lambda}_n(\tilde{\mathbf{r}}')\frac{1}{|\mathbf{r}-\tilde{\mathbf{r}}'|^3}dS'. \tag{22}$$

observing that $\mathcal{J}(\boldsymbol{\xi}_0)$ is simply twice the area of the flat tangent triangle $\mathcal{T}'_T$. Hence, the integral (22) is basically the integral (6) defined over the tangential triangle $\mathcal{T}'_T$, and can be analytically evaluated as in [3].

By contrast, the integral (19) is still defined over the initial curvilinear domain, and exhibits an asymptotic behavior $1/R$ for $R \to 0$; it can be evaluated by applying the radial-angular transform. In order to apply the radial-angular transform to a curvilinear integration domain, the associated flat tangent triangle $\mathcal{T}'_T$ is divided into sub-triangles about the projected observation point, and the radial-angular transform is applied to each tangent sub-triangle (as described in Sect. II). The quadrature sample points, obtained in (u, v) coordinates (10), may be mapped back to the tangent sub-triangle, and then back to the simplex (in $\boldsymbol{\xi}$ coordinates), as shown in Fig. 3b. Finally, the simplex quadrature sample points in $\boldsymbol{\xi}$ coordinates may be mapped to the initial curvilinear integration domain via (14). The procedure is graphically described in Fig. 5.

IV. Numerical Results

In order to analyze the accuracy of the proposed hybrid integration scheme, we analyze the convergence behavior of the integral (1) for different observation points $\mathbf{r}$ for both flat and curvilinear integration domains.

The proposed integration scheme, labelled in the following as "RA-1", is compared with the fully numerical singularity cancellation scheme in [8], devoted to strongly near-singular integrals and labelled as "SC", and with a standard singularity subtraction scheme for integrals of the kind in (1), labelled as "SS" [3]. The quadrature rules used to integrate the difference integrands are Gauss-Legendre (GL) for the SC scheme, Gauss-Triangle (GT) [23] for the SS scheme

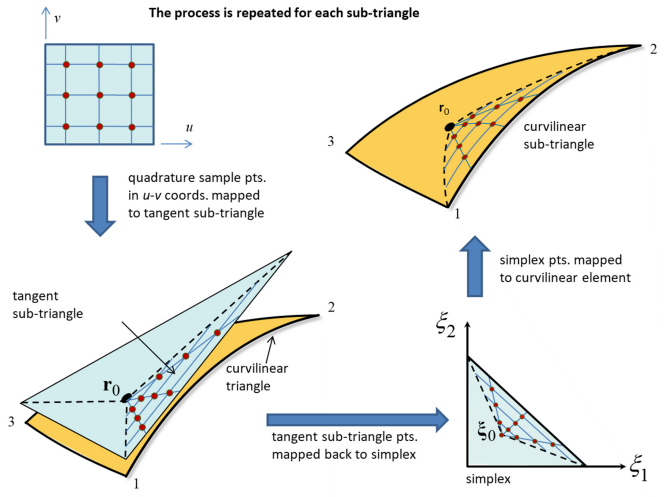

Fig. 5. Pictorial description of the procedure to apply radial-angular transform to a curvilinear integration domain.

(using a binary/dyadic division of the triangle for more than 166 points), and for the RA-1 scheme GL and Ma-Rokhlin-Wandzura [24]–[26] with square root weighting (MRWsqrt) . In the case of the RA-1 scheme, if the observation point lies in the triangular integration domain, the GL quadrature rule is used; otherwise (i.e., observation point not in the plane of the (tangent) triangle), a MRWsqrt quadrature rule is used for the radial integration and a GL quadrature is used for transverse integration in the radial angular scheme [19].

The reference values are obtained applying the RA-1 scheme and using the highest order available for GL and MRWsqrt quadrature rules, with 166 and 128 sample points, respectively. The reference values are evaluated in quad precision, and they are accurate to no less than 16 significant digits.

In all the reported numerical results, the integration domain is a triangle with maximum edge of about $\lambda/5$ (where λ is the working wavelength), and the chosen basis functions are RWG basis functions (2) on flat triangles or their extension to curvilinear (quadratic) triangles (15). The integral evaluation accuracy is measured in terms of the number of correct significant digits of the computed integral,

$$\mathrm{SD}_{n,\alpha}(i) = -\log\left(\left|\frac{I^{\mathrm{ref}}_{n,\alpha} - I_{n,\alpha}(i)}{I^{\mathrm{ref}}_{n,\alpha}}\right| + \delta\right), \qquad (23)$$

where α is the considered integral component (tangential or normal to the integration domain at $\mathbf{r}_0$), $I^{\mathrm{ref}}_{n,\alpha}$ and $I_{n,\alpha}(i)$ is the α-component of the evaluated integral with the highest available number of quadrature sample points (reference) and with i quadrature sample points, respectively. The term $\delta = 10^{-16}$ is inserted in (23) to limit the precision claim to 16 digits (double precision). In all the following graphs, the obtained $\mathrm{SD}_{n,\alpha}(i)$ are reported with respect to the number of quadrature sample points per dimension, i.e., equal to $\sqrt{i}$ since we are performing a 2-D surface integral. We do not include timing analyses since, as verified, run-times are mainly dominated by the number of sample points in each scheme.

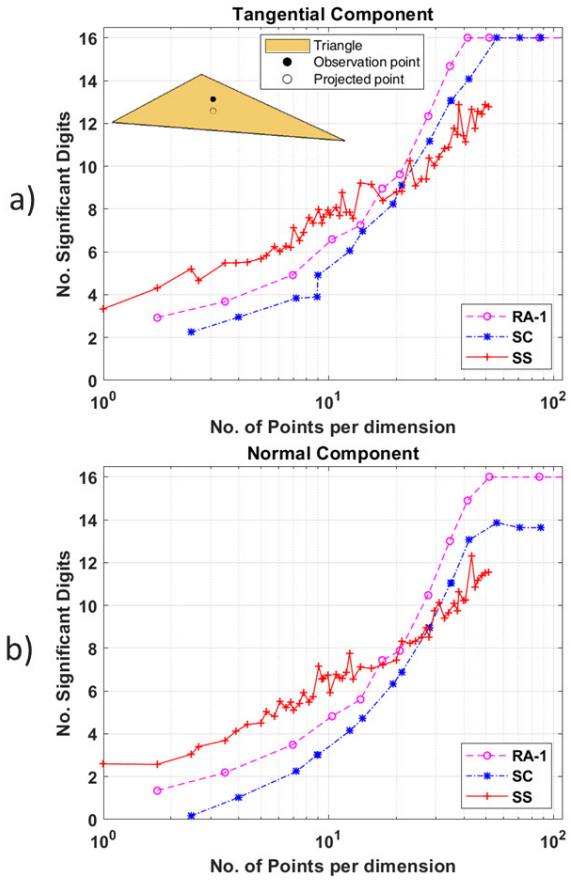

Fig. 6. No. of correct significant digits versus the no. of quadrature sample points per dimension; case of a flat triangle with observation point $\lambda/100$ off the triangular surface projected close to the triangle centroid (inset); (a): integral tangential component; (b): integral normal component.

Figure 6 shows the accuracy in the evaluation of the integral (1) in the case of a flat integration domain, and with the observation point $\mathbf{r}$ placed at a distance of $\lambda/100$ from the triangular surface and projected close to the triangle centroid (see the inset of Fig. 6). The obtained number of correct significant digits with respect to the number of quadrature sample points per dimension confirms the expected behavior of the different integration schemes. The singularity subtraction scheme (solid red line with plus sign) shows fairly good accuracy for a low-to-medium number of quadrature sample points, and converges slower to machine precision with respect to the other schemes . The singularity cancellation scheme (dash-dotted blue line with filled square) nearly reaches machine precision as the number of quadrature points increases, but, for a low-to-medium number of quadrature points, its accuracy is significantly below the performance of the singularity subtraction scheme. The proposed hybrid integration scheme (dashed magenta line with hollow circles), on the other hand, displays low-to-medium accuracy with only about one digit less accuracy than the singularity subtraction scheme (up to 7-8 digits), but converges faster to machine precision (16 digits) than the singularity cancellation and singularity subtraction schemes.

Figure 7 reports, for the same triangle as in Fig. 6, the

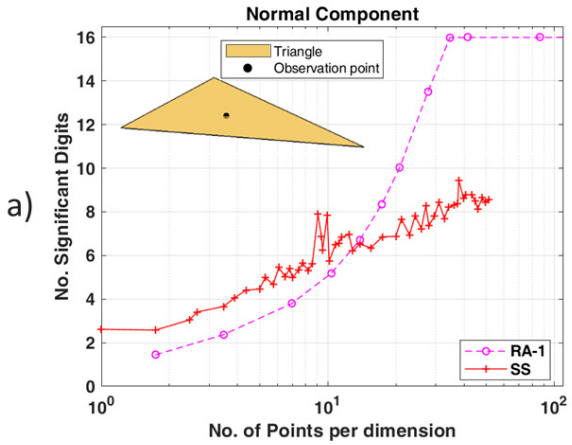

Fig. 7. No. of correct significant digits of the integral normal component versus the no. of quadrature sample points per dimension; case of a flat triangle with observation point on the triangular surface at around the triangle centroid (inset).

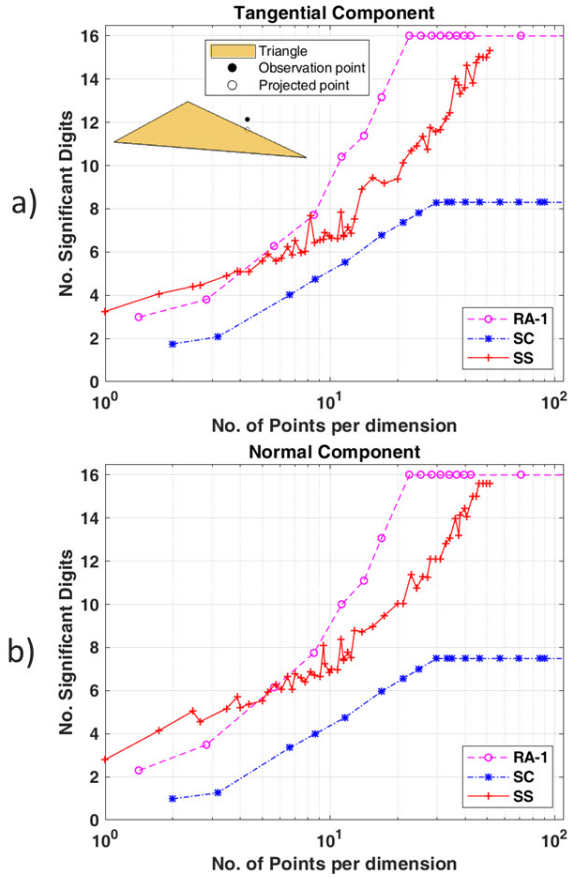

Fig. 8. No. of correct significant digits versus the no. of quadrature sample points per dimension; case of a flat triangle with observation point $\lambda/100$ off the triangular surface projected on one triangle edge (inset); (a): integral tangential component; (b): integral normal component.

integral evaluation accuracy when the observation point is *on* the triangular surface close to the triangle centroid (inset of Fig. 7). In this case, only the normal component of the integral is non-vanishing, and the singularity cancellation scheme is not applicable because it requires a finite distance between the observation point and the integration domain. The behavior of the proposed hybrid integration scheme is similar to the previous case, i.e. it is comparable with the singularity subtraction scheme up to 7-8 significant digits and is able to reach machine precision at faster pace. This result demonstrates the consistency of the proposed integration scheme for the limiting case of an observation point exactly on the surface of the triangle.

A case of special interest is that of an observation point close to the integration domain edges or projecting directly onto an edge (see the inset of Fig. 8). This case is often critical for numerical integration schemes, and leads to an integral with a bounded normal component, but with higher order singularities [24]. As shown in Fig. 8, in this case, the accuracy of the singularity cancellation scheme [8] is limited to around 8 significant digits, because the disc, that is one of the sub-domains into which the initial integration domain is divided, is not a full disc, losing the advantage of symmetry. Instead, the proposed hybrid integration schemes improves both achievable accuracy and convergence compared to the previous case.

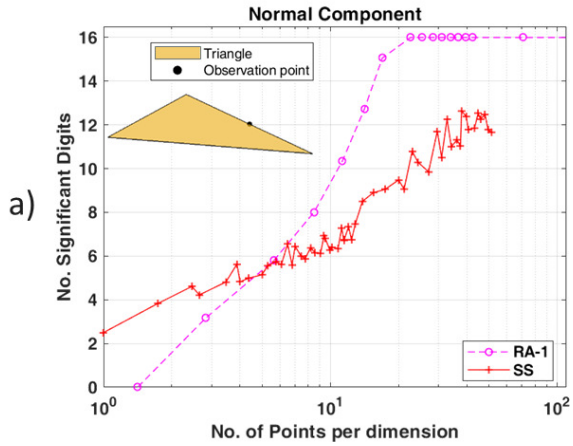

Fig. 9. No. of correct significant digits of the integral normal component versus the no. of quadrature sample points per dimension; case of a flat triangle with observation point on one triangle edge (inset).

Finally, we consider the case of an observation point directly on the triangle edge, as shown in the inset of Fig. 9. In this case, the exact contribution integral (6) is unbounded and, hence, its contribution has been excluded from the results reported in Fig. 9. Nevertheless, the accuracy of the proposed hybrid integration scheme is fully analogous to that reported in Fig. 8, demonstrating that the fully numerical part of the scheme is stable even when the observation point is on an edge of the integration domain.

To demonstrate the applicability of the proposed hybrid integration scheme to *curvilinear* (quadratic) triangles, in Figs. 10–13, we report the same analyses done for flat integration domains, for the case of curvilinear domains (see inset of

Figs. 10–13). We observe that, in the implemented singularity subtraction scheme, in the case of a curvilinear integration domain, the asymptotic terms for $R \to 0$ [3] are analytically evaluated on the corresponding flat tangent triangle, in an analogous way as for the proposed hybrid integration scheme (19), (20).

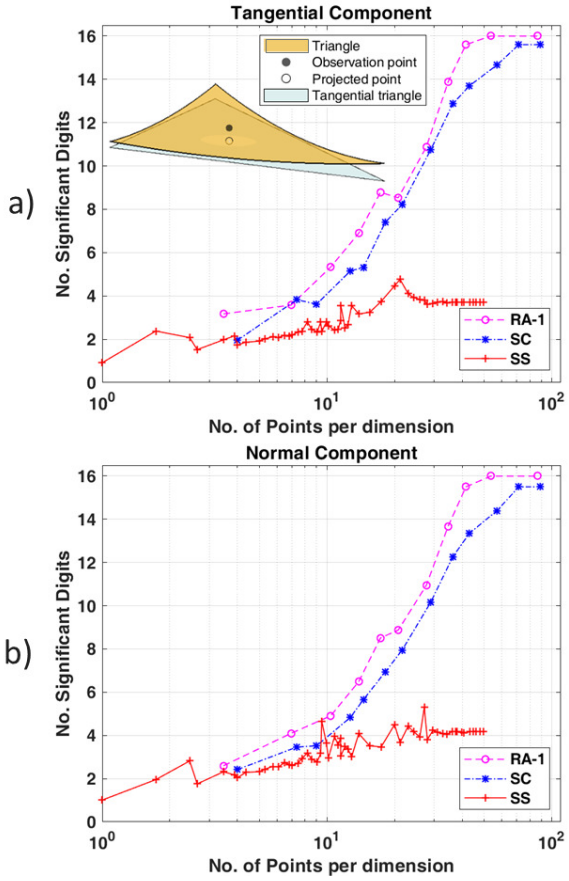

Fig. 10. No. of correct significant digits versus the no. of quadrature sample points per dimension; case of a curvilinear triangle with observation point $\lambda/100$ off the triangular surface projected close to the triangle centroid (inset); (a): integral tangential component; (b): integral normal component.

Figure 10 shows the convergence of the integral (1) for a curvilinear triangular domain with the observation point chosen at a distance of $\lambda/100$ from the triangular surface; the observation point projection lies close to the centroid of the triangle (see the inset of Fig. 10). The behaviors of the proposed hybrid integration scheme and the singularity cancellation scheme are similar to those shown in Fig. 6 for the flat triangle. On the other hand, the singularity subtraction scheme shows significantly poorer convergence, probably because the subtracted and added asymptotic terms are not able to sufficiently smooth the integrand for accurate numerical integration on the curvilinear domain.

Figure 11 illustrates the case of an observation point on the curvilinear triangular surface, close to its centroid. Here, as for the planar case, it is not possible to use the singularity cancellation scheme [8], because it requires a finite distance between the observation point and the integration domain. Therefore, only the proposed hybrid integration and singularity

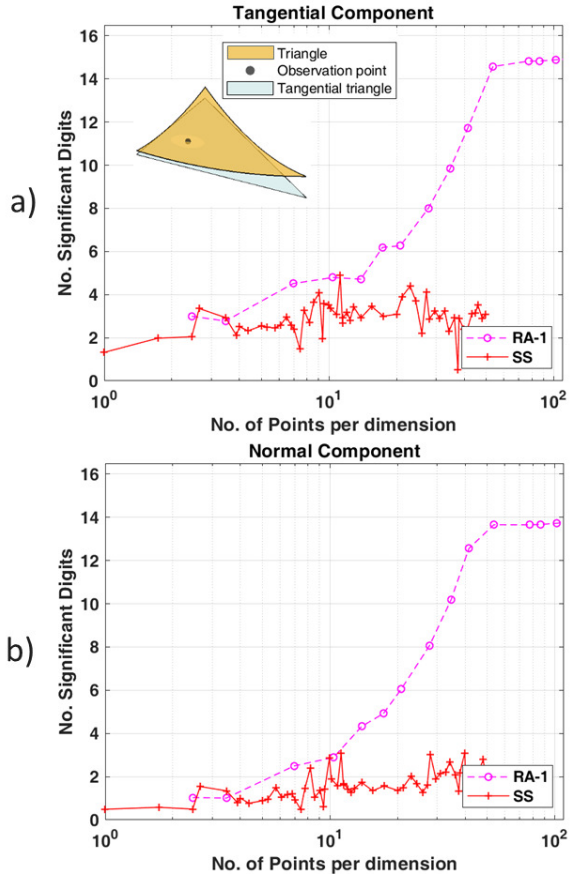

Fig. 11. No. of correct significant digits versus the no. of quadrature sample points per dimension; case of a curvilinear triangle with observation point on the triangular surface at around the triangle centroid (inset); (a): integral tangential component; (b): integral normal component.

subtraction schemes are compared here. The behaviour of the hybrid integration scheme is similar to that for the corresponding flat case (see Fig. 7), even though here both integral components are present since the tangential one is no longer zero; moreover, it outperforms the singularity subtraction scheme.

In Fig. 12, the case of a curvilinear triangle with an observation point projected onto a triangle edge is reported. As in the case of flat triangles (see Fig. 8), the accuracy achieved by the singularity cancellation scheme is limited due to the radial half-disc integration issue. By contrast, the proposed hybrid integration scheme is able to reach machine precision merely by increasing the number of quadrature sample points, and with better accuracy than the singularity subtraction scheme.

Finally, to demonstrate the stability of the proposed hybrid integration scheme, in Fig. 13, we analyze a limiting case in which the observation point is on the edge of the curvilinear triangle. In this case, as for the flat triangle, the analytical integration (6) is infinite, and therefore only the numerical integral is reported in the graph. The convergence behavior is similar to that of previous case, demonstrating the stability of the hybrid integration scheme as the observation point approaches the integration surface.

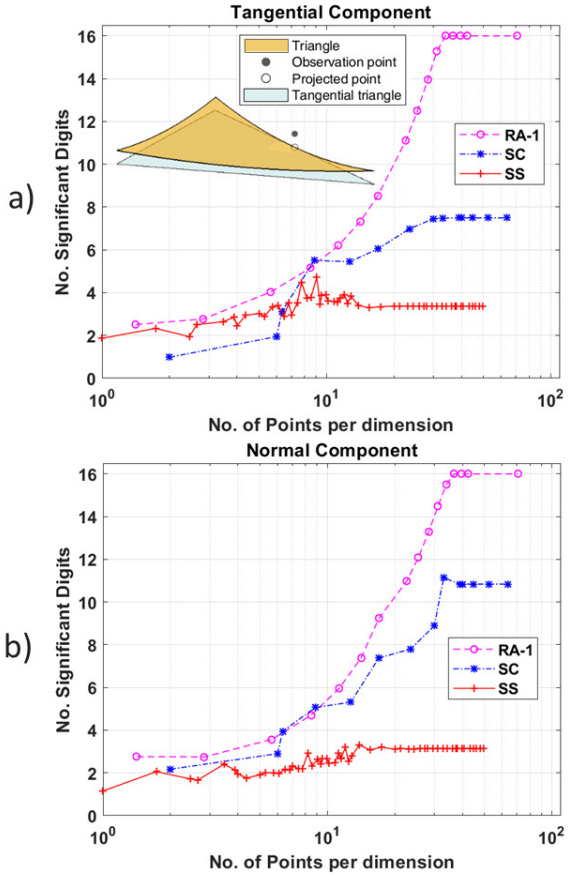

Fig. 12. No. of correct significant digits versus the no. of quadrature sample points per dimension; case of a curvilinear triangle with observation point $\lambda/100$ off the triangular surface projected on one triangle edge (inset); (a): integral tangential component; (b): integral normal component.

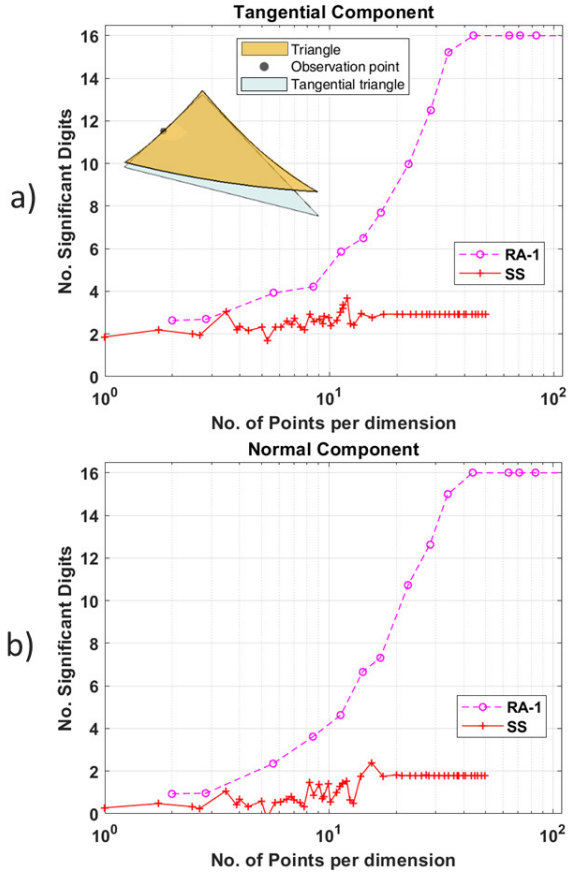

Fig. 13. No. of correct significant digits versus the no. of quadrature sample points per dimension; case of a curvilinear triangle with observation point on the triangle edge (inset); (a): integral tangential component; (b): integral normal component.

V. Conclusion and Perspectives

We have proposed an integration scheme that properly combines the singularity cancellation and singularity subtraction schemes for the evaluation of surface integrals involving the gradient of the Green's function, such as appear in the MoM discretization of the MFIE. The proposed method consists of the subtraction of one asymptotic term, to reduce the order of the kernel singularity as $R \to 0$, and, together with an appropriate variable transformation, evaluating the remaining singular or near-singular integrand numerically. The method is simple to implement, and its numerical behavior replicates the desirable features of the two schemes on which it is based, i.e. it exhibits good accuracy for a low-to-medium number of quadrature sample points and rapid convergence to machine precision as the number of quadrature points is increased. It is demonstrated that the method applies to both flat and curvilinear (quadratic) triangles and for observation points close to or exactly on the integration surface or edges. The next step of the research activity is to apply the proposed approach to higher order basis functions. Moreover, the method would benefit from the implementation of an optimization algorithm for the numerical integral to automatically select the appropriate number of points for a given precision, as proposed for the radial-angular scheme applied to $1/R$ singularities in [19].

References

[1] W. C. Chew, M. S. Tong, and B. Hu, "Integral Equation Methods for Electromagnetic and Elastic Waves," *Synthesis Lectures on Computational Electromagnetics*, vol. 3, no. 1, pp. 1–241, 2008.

[2] P. Ylä-Oijala, M. Taskinen, and S. Järvenpää, "Surface Integral Equation Formulations for Solving Electromagnetic Scattering Problems with Iterative Methods," *Radio Sci.*, vol. 40, no. 6, p. RS6002, Dec. 2005. [Online]. Available: http://doi.wiley.com/10.1029/2004RS003169

[3] R. Graglia, "On the Numerical Integration of the Linear Shape Functions Times the 3-D Green's Function or its Gradient on a Plane Triangle," *IEEE Transactions on Antennas and Propagation*, vol. 41, no. 10, pp. 1448–1455, Oct. 1993.

[4] S. Järvenpää, M. Taskinen, and P. Ylä-Oijala, "Singularity Subtraction Technique for High-Order Polynomial Vector Basis Functions on Planar Triangles," *IEEE Transactions on Antennas and Propagation*, vol. 54, no. 1, pp. 42–49, Jan. 2006.

[5] J. Rivero, F. Vipiana, J. M. Taboada, D. R. Wilton, and W. A. Johnson, "Comparison of Different Schemes for Dealing with Integral Singularities in Method of Moments," in *IEEE International Symposium on Antennas and Propagation*, San Diego, CA, US, 2017.

[6] L. Li and T. F. Eibert, "Radial-Angular Singularity Cancellation Transformations Derived by Variable Separation," *IEEE Transactions on Antennas and Propagation*, vol. 64, pp. 189–200, Jan. 2016.

[7] M. Botha, "Numerical Integration Scheme for the Near-Singular Green Function Gradient on General Triangles," *IEEE Transactions on Antennas and Propagation*, vol. 63, no. 10, pp. 4435–4445, Oct. 2015.

[8] F. Vipiana and D. R. Wilton, "Numerical Evaluation via Singularity Cancellation Schemes of Near-Singular Integrals Involving the Gradient of Helmholtz-Type Potentials," *IEEE Transactions on Antennas and Propagation*, vol. 61, no. 3, pp. 1255–1265, Mar. 2013.

[9] P. W. Fink and M. A. Khayat, "A Simple Transformation for the Numerical Evaluation of Near Strongly Singular Integrals," *IEEE*

Antennas and Wireless Propagation Letters, vol. 12, pp. 225–228, 2013. [Online]. Available: http://ieeexplore.ieee.org/document/6420865/

[10] J. Rivero, F. Vipiana, D. R. Wilton, and W. A. Johnson, "Evaluation of 4-D Reaction Integrals Via Double Application of the Divergence Theorem," *IEEE Transactions on Antennas and Propagation*, vol. 67, no. 2, pp. 1131–1142, Feb. 2019.

[11] E. Bleszynski, M. Bleszynski, and T. Jaroszewicz, "Reduction of Singular Surface Integrals to Non-Singular Line Integrals for Matrix Elements of Tensor and Vector Green Functions for Arbitrarily Oriented Pairs of Flat Surface elements," in *The 12th European Conference on Antennas and Propagation*, London, UK, 2018.

[12] D. Tihon and C. Craeye, "All-Analytical Evaluation of the Singular Integrals Involved in the Method of Moments," *IEEE Transactions on Antennas and Propagation*, vol. 66, no. 4, pp. 1925–1936, Apr. 2018.

[13] D. Wilton, F. Vipiana, and W. Johnson, "Evaluation of 4-D Reaction Integrals in the Method of Moments: Co-planar Element Case," *IEEE Transactions on Antennas and Propagation*, vol. 65, no. 5, pp. 2479–2493, May 2017.

[14] E. H. Bleszynski, M. K. Bleszynski, and T. Jaroszewicz, "Reduction of Singular Surface Integrals to Nonsingular Line Integrals in Integral Equations for Planar Geometries," *IEEE Transactions on Antennas and Propagation*, vol. 64, no. 11, pp. 4760–4769, Nov. 2016.

[15] A. G. Polimeridis, F. Vipiana, J. R. Mosig, and D. R. Wilton, "DIRECTFN: Fully Numerical Algorithms for High Precision Computation of Singular Integrals in Galerkin SIE Methods," *IEEE Transactions on Antennas and Propagation*, vol. 61, no. 6, pp. 3112–3122, Jun. 2013.

[16] M. S. Tong and W. C. Chew, "A Novel Approach for Evaluating Hypersingular and Strongly Singular Surface Integrals in Electromagnetics," *IEEE Transactions on Antennas and Propagation*, vol. 58, no. 11, pp. 3593–3601, Nov. 2010.

[17] J. Rivero, F. Vipiana, D. R. Wilton, and W. A. Johnson, "A Hybrid Integration Scheme to Handle Singularities in the MFIE," in *IEEE International Symposium on Antennas and Propagation*, Boston, MA, US, 2018.

[18] S. Rao, D. Wilton, and A. Glisson, "Electromagnetic Scattering by Surfaces of Arbitrary Shape," *IEEE Transactions on Antennas and Propagation*, vol. 30, no. 3, pp. 409–418, May 1982.

[19] M. A. Khayat, D. R. Wilton, and P. W. Fink, "An Improved Transformation and Optimized Sampling Scheme for the Numerical Evaluation of Singular and Near-Singular Potentials," *IEEE Antennas and Wireless Propagation Letters*, vol. 7, pp. 377–380, 2008.

[20] M. M. Botha, "A Family of Augmented Duffy Transformations for Near-Singularity Cancellation Quadrature," *IEEE Transactions on Antennas and Propagation*, vol. 61, pp. 3123–3134, June 2013.

[21] R. D. Graglia, D. R. Wilton, and A. F. Peterson, "Higher Order Interpolatory Vector Bases for Computational Electromagnetics," *IEEE Transactions on Antennas and Propagation*, vol. 45, pp. 329–342, Mar. 1997.

[22] D. R. Wilton, F. Vipiana, and W. A. Johnson, "Evaluating Singular, Near-Singular, and Non-Singular Integrals on Curvilinear Elements," *Electromagnetics*, vol. 34, no. 3-4, pp. 307–327, Apr. 2014.

[23] L. Zhang, T. Cui, and H. Liu, "A Set of Symmetric Quadrature Rules on Triangles and Tetrahedra," *Journal of Computational Mathematics*, vol. 27, no. 1, pp. 89–96, 2009.

[24] F. Vipiana, D. R. Wilton, and W. A. Johnson, "Advanced Numerical Schemes for the Accurate Evaluation of 4-D Reaction Integrals in the Method of Moments," *IEEE Transactions on Antennas and Propagation*, vol. 61, no. 11, pp. 5559–5566, Nov. 2013.

[25] J. Ma, V. Rokhlin, and S. Wandzura, "Generalized Gaussian Quadrature Rules for Systems of Arbitrary Functions," *SIAM Journal on Numerical Analysis*, vol. 33, no. 3, pp. 971–996, 1996. [Online]. Available: http://www.jstor.org/stable/2158491

[26] ——, "Generalized Gaussian Quadrature Rules for Systems of Arbitrary Functions," Yale University, New Haven, CT, USA., Dept. Computer Science, Tech. Rep. YALEU/DCS/RR-990, Oct. 1993.

Javier Rivero received the M.S. Telecommunication Engineering degree at University Carlos III de Madrid, Spain in 2008 and the Ph.D. in Telecommunication Engineering from University of Extremadura, Spain in 2012. From 2012 to 2017 he was a research assistant at the Department of Technologies of Computers and Communications at University of Extremadura, Spain. From 2015 to 2017 he did a postdoctoral stay at the Department of Electronics and Telecommunications of Politecnico di Torino. From 2017 to 2018 he was at the Advanced Computing and Electromagnetics (ACE) of Istituto Superiore Mario Boella (ISMB). Since 2018, he has been a research assistant with the Department of Electronics and Telecommunications, Politecnico di Torino.

His current research interests include fast integral-equation methods and method of moment approaches in computational electromagnetics, metamaterials, nanoplasmonics, Greens function regularization, and advanced quadrature integration schemes.

Francesca Vipiana (M'07–SM'13) received the Laurea and Ph.D. degrees in electronic engineering from the Politecnico di Torino, Torino, Italy, in 2000 and 2004, respectively, with doctoral research carried out partly at the European Space Research Technology Center, Noordwijk, The Netherlands. From 2005 to 2008, she was a Research Fellow with the Department of Electronics, Politecnico di Torino. From 2009 to 2012, she was the Head of the Antenna and EMC Lab with the Istituto Superiore Mario Boella, Torino. Since 2012, she has been an Assistant Professor with the Department of Electronics and Telecommunications, Politecnico di Torino, where she has been an Associate Professor since 2014. Her current research interests include numerical techniques based on the integral equation and method of moment approaches, with a focus on multiresolution and hierarchical schemes, domain decomposition, preconditioning and fast solution methods, and advanced quadrature integration schemes. Prof. Vipiana received the Young Scientist Award at the URSI General Assembly in 2005, the first prize in the poster competition at the IEEE Women in Electromagnetics Workshop in 2009, the ISMB Best Paper Award in 2011, and the Lot Shafai Mid-Career Distinguished Award from the IEEE Antennas and Propagation Society in 2017.

Donald R. Wilton (S'63–M'65–SM'80–F'87–LF'08) received the B.S., M.S., and Ph.D. degrees in Electrical Engineering from the University of Illinois, Urbana-Champaign, in 1964, 1966, and 1970, respectively. From 1965 to 1968 he was with Hughes Aircraft Co., Fullerton, CA, engaged in the analysis and design of phased array antennas. From 1969 to 1970, he pursued the Ph.D. under a Hughes Doctoral Fellowship. From 1970–1983 he was with the Department of Electrical Engineering, University of Mississippi. He was a Visiting Professor at Syracuse University during the academic year 1978–1979. He was with the University of Houston from 1983 until 2012, retiring as Professor Emeritus in the Department of Electrical and Computer Engineering. During the 2004–2005 academic year he was a visiting professor at the Polytechnic of Turin, Italy, Sandia National Laboratories, and the University of Washington. His primary research area is computational electromagnetics, and he has published, lectured, and consulted extensively in this area. Dr. Wilton is a Life Fellow of the IEEE and received the IEEE Third Millennium Medal. He has served the IEEE Antennas and Propagation Society as an Associate Editor of the Transactions on Antennas and Propagation, as a Distinguished National Lecturer, and as a member of its Administrative Committee. He is also a member of URSI Commission B, in which he has held various offices, including Chair of US Commission B. Dr. Wilton received the ACES inaugural Computational Electromagnetic Award in 2013, the IEEE Antenna and Propagation Society's inaugural Harrington-Mittra Award in Computational Electromagnetics in 2014, and the 2015 IEEE Electromagnetics Award.

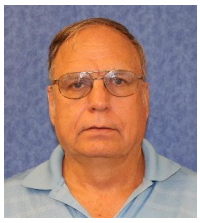

William A. Johnson (M'00–SM'02) received the B. S., M. A., and Ph. D. degrees in mathematics with minors in physics from the University of Arizona, Tucson, AZ, in 1972, 1974, and 1978, respectively. The Ph. D. degree was obtained in association with the Interdisciplinary Applied Math program at the University of Arizona. He is the author/co-author of 41 journal articles. His work experience includes Sandia National Laboratories, Lawrence Livermore National Laboratory, University of Mississippi, and adjunct associate professor of mathematics at the University of New Mexico. He was a visiting assistant professor of mathematics at New Mexico Institute of Mining and Technology, in Socorro New Mexico for the 2016-2107 academic year. Dr. Johnson is a full member of URSI Commission B and a Senior Member of the IEEE. New Mexico Tech is gratefully acknowledged for providing this photo.